Development of Crystalline Structure during Tubular Film Blowing of Low-Density Polyethylene

TAE HOON KWACK* and CHANG DAE HAN,† *Department of Chemical Engineering, Polytechnic University, Brooklyn, New York 11201* and M. E. VICKERS, *Research Center, British Petroleum Inc., Chertsey Road, Sunbury-on-Thames, Middlesex, TW16 7LN, United Kingdom*

Synopsis

Development of crystalline structure during the tubular film blowing of low-density polyethylene was investigated, using wide-angle X-ray diffraction technique, low-angle light scattering, and scanning electron microscopy. In the study, commercial grades of both high-pressure low-density polyethylene (HP-LDPE) and low-pressure low-density polyethylene (LP-LDPE) (also, commonly referred to as linear low-density polyethylene, LLDPE) were used. The applied stresses at the freeze line were determined using theoretical expressions derived in an earlier publication [C. D. Han and T. H. Kwack, *J. Appl. Polym. Sci.*, **28**, 3399 (1983)]. The applied stresses, S_{11F} and S_{33F}, at and above the freeze line in the machine and transverse directions were expressed in terms of the tension at the take-up device, take-up ratio, blow-up ratio, and the pressure difference across the film of the bubble. These applied stresses were used to interpret the crystalline axes' orientation in the tubular blown films. It was found that the magnitude of S_{11F} is an important process parameter for the crystalline axes' orientation and that the biaxial stress ratio (S_{11F}/S_{33F}) appears to be a determining factor in the distribution of fibrillous nuclei and crystalline texture, as well as film anisotropy.

INTRODUCTION

In film blowing operations, the macromolecules that undergo shear deformation inside a tubular die reorient themselves upon exiting from the die under biaxial stretching. Biaxial stretching is realized by stretching the tubular bubble simultaneously in the machine direction (MD) with a take-up device, and in the transverse direction (TD) by bubble inflation. Figure 1 gives a schematic depicting the process. Depending upon the extent of stretching in the MD and TD and, also, the temperature at which the material is stretched, the degree of molecular orientation in the blown bubble varies.

In the past, some serious attempts were made to achieve a better understanding of the tubular film blowing process from the point of view of fluid mechanics,[1,2] elongational flow,[3-5] bubble stability,[6,7] and the mechanical/physical properties of the films, as affected by processing variables.[8,9]

Today, it is a well-established fact that the molecular orientation and crystalline structure in a fabricated polymer product greatly influence its

*Presently with Mobil Chemical Company, Technical Center, Macedon, NY 14502.
†To whom correspondence should be addressed.

Journal of Applied Polymer Science, Vol. 35, 363–389 (1988)

CCC 0021-8995/88/020363-27$04.00

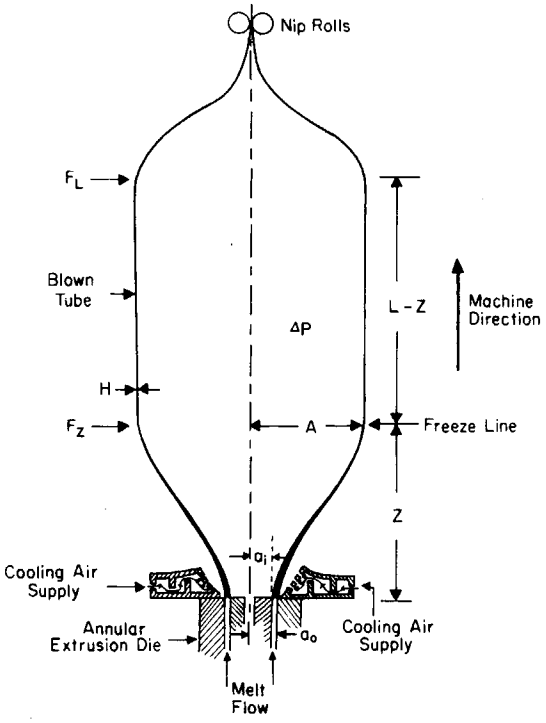

Fig. 1. Schematic describing the film blowing process.

mechanical/physical properties. When dealing with partially crystalline polymers, the orientation of crystallites and the orientation of the amorphous region are equally important in obtaining the mechanical/physical properties desired. The tubular film blowing process has been in existence for over two decades. During this time, some serious attempts have been made to investigate the relationship between the molecular orientation and the mechanical properties of tubular blown film.[10-17] Holmes and Palmer[10] and Aggarwal et al.[11] have reported that the *a*-axis of the crystalline phase in polyethylene blown film is oriented along the MD, while the *b*- and *c*-axes are randomly distributed in the plane perpendicular to the *a*-axis. However, Lindenmeyer and Lustig[12] favor the mechanism of "row orientation," first proposed by Keller and Machin.[18] In "row orientation," the *b*-axis of the crystalline phase is the preferred orientation. It is perpendicular to the MD while the *a*- and *c*-axes are randomly distributed with cylindrical symmetry about it. On the basis of X-ray pole figure measurements, Desper[13] suggested a "modified row orientation" structure. It appears that these different proposed mechanisms of structure development may stem from film samples prepared under different processing conditions.

Until the recent studies by White and co-workers[19-21] and Maddams and Vickers,[22] the earlier investigators[10-17] paid little attention to how the property–morphology relationships obtained were affected by the processsing conditions employed to obtain the film specimens they examined. White and co-workers investigated the effects of processing variables on the orientation

development during the tubular film blowing of polystyrene,[19] high-density polyethylene,[20] and polypropylene.[21] In their study, they correlated the birefringence to both the take-up ratio and the applied stresses at vitrification for polystyrene tubular films.[19] They also correlated the crystalline orientation factors and the birefringence to the take-up ratio and the applied stresses at the freeze line for high-density polyethylene and polypropylene.[20,21] Maddams and Vickers[22] correlated the crystalline axes' orientation of high-density polyethylene film to the cooling rate and elongation rate. Recently, Ashizawa et al.[23] reported that little variation existed in the crystalline orientation with changes in blow-up ratio or take-up ratio for the high-pressure and low-pressure low-density polyethylenes that they investigated.

As part of a continuing effort towards achieving a better understanding of rheology–processing–property–morphology relationships in tubular film blowing, we have conducted an investigation on the development of crystalline structure during the tubular film blowing of low-density polyethylene, both high-pressure low-density polyethylene (HP-LDPE) and low-pressure low-density polyethylene, commonly referred to as linear low-density polyethylene (LLDPE). Emphasis was placed on investigating the effects of processing conditions on the resulting crystalline structure of the film samples that we examined. In this paper, we will report the highlights of our findings.

EXPERIMENTAL

Materials

A high-pressure low-density polyethylene (HP-LDPE) (Union Carbide Corp.) and a linear low-density polyethylene (LLDPE) (Mitsui Petrochemical) were used in this study. It is believed that the Mitsui LLDPE was produced by solution polymerization and that it is a copolymer of ethylene and 4-methyl pentene-1. Information on molecular weight, molecular weight distribution, and other molecular parameters are given in Table I. The rheological properties of these polymers have been reported in previous publications.[24,25]

Apparatus and Procedures

The apparatus and procedures employed for obtaining film samples are the same as those described in a previous paper.[24] During the film blowing experiment, the following variables were measured: (a) the tension, using a Bar Tensiometer (Tensitron Co.); (b) the air pressure inside the tubular bubble, using a water manometer; (c) the temperature and flow rate of the

TABLE I
Molecular Characteristics Data of HP-LDPE and LLDPE Employed

Resin	Density	Melt index	$\bar{M}_n$	$\bar{M}_w$	$\bar{M}_w/\bar{M}_n$	λ_n[a]
HP-LDPE	0.918	2.0	2.13×10^4	2.01×10^5	9.43	3.4
LLDPE	0.921	2.0	5.60×10^4	2.21×10^5	3.95	—

[a] λ_n represents the long-chain branching frequency defined as the number-average number of branch points per 1000 carbon atoms.

TABLE II
Processing Conditions and Calculated Values of S_{11F} and S_{33F} for Blown Film Specimens

Resin	Sample no.	Melt extrusion temperature (°C)	Cooling air flow rate (cm^3/sec)	BUR	TUR	$S_{11F} \times 10^{-5}$ (Pa)	$S_{33F} \times 10^{-5}$ (Pa)	S_{11F}/S_{33F}
HP-LDPE	1	200	2210	1.45	3.98	1.48	0.10	14.12
	2	200	2210	1.63	3.98	1.56	0.13	11.75
	3	200	2210	2.75	3.98	1.71	0.34	4.95
	4	200	2210	3.26	3.98	1.86	0.48	3.84
	5	200	2210	2.88	9.86	4.45	0.77	5.78
	6	200	2210	2.88	15.61	7.43	0.95	7.84
	7	200	2210	1.68	21.44	8.80	0.57	15.47
	8	200	2210	2.25	21.44	9.01	0.90	9.93
	9	200	2210	2.83	21.44	9.84	1.25	7.84
	10	200	2210	4.13	21.44	11.29	2.29	4.93
LLDPE	11	220	2883	3.06	7.9	1.35	0.90	1.49
	12	220	2883	2.96	11.4	2.11	1.11	1.89
	13	220	2883	3.13	14.7	2.77	1.32	2.10
	14	220	2883	3.00	18.0	3.25	1.33	2.46

cooling air; (d) the mass flow rate of molten polymer (and hence the linear velocity of the melt at the die lip); (e) the melt temperature; (f) the diameter of the tubular bubble; (g) the position of the freeze line; (h) the thickness of the tubular film. These measurements allowed us to calculate the imposed stresses in the film at the freeze line, in both the machine direction (MD) and transverse direction (TD). The calculation of stresses has enabled us to relate the processing conditions to the crystalline structure and mechanical properties of the tubular blown films produced.

Wide-Angle X-Ray Diffraction

Flat plate photographs of wide-angle X-ray diffraction patterns of 14 blown film specimens (see Table II) were taken at 35 kV and 12 mA with nickel filtered CuK_α radiation using a Statton camera. Samples were photographed, under a helium atmosphere, from three perpendicular directions, namely, the MD, TD, and neutral direction (ND). Pole figures of (200) and (020) planes were obtained for selected samples, using a Schultz Texture Goniometer in the reflection mode, with automatic data collection. The pole figures were plotted with corrections for absorption and defocusing.

Small-Angle Light Scattering

Small-angle light scattering patterns of blown film specimens were collected on Polaroid 57 film using an apparatus analogous to the one described by Stein.[26] A plane polarized Spectra-Physics He–Ne laser was used as a light source. Specimens were placed such that the film surface was normal to the laser beam and the machine direction of the film was parallel to the polarization direction of the polarizer.

Tensile and Dynamic Mechanical Properties Measurement

Tensile properties of the film specimens were measured at room temperature, using an Instron testing machine. Measurements of several samples collected under identical processing conditions were taken, and the average value was used to plot the data.

Dynamic mechanical properties of the specimens, namely, elastic modulus and loss tangent ($\tan\delta$), were determined using a Rheovibron Viscoelastometer DDV-II at a frequency of 3.5 Hz.

RESULTS AND DISCUSSION

Tensile Stress at the Freeze Line as Affected by Processing Variables

In reference to Figure 1, let us now define two dimensionless parameters, blow-up ratio (BUR) and take-up ratio (TUR), by

$$\text{BUR} = A/a_o \tag{1}$$

$$\text{TUR} = V/v_o \tag{2}$$

where A is the radius of the tubular bubble at the freeze line, a_o is the outer radius of the die, V is the linear velocity of the tubular bubble at the freeze line (i.e., the take-up speed), and v_o is the linear average velocity of the melt at the die exit.

In the film blowing process, the stresses, S_{11F} and S_{33F}, at the freeze line in the MD and TD, respectively, may be calculated by[24]

$$S_{11F} = \frac{F_L}{C}\frac{\rho_s}{\rho_m}(\text{TUR}) - \rho_s g(L - Z) \tag{3}$$

$$S_{33F} = \frac{1}{B}\frac{\rho_s}{\rho_m}(\Delta p)(\text{BUR})^2(\text{TUR}) \tag{4}$$

where F_L is the tension measured at a distance L above the die exit, ρ_s and ρ_m are the densities of the solidified film and melt, respectively, Δp is the pressure difference across the film of the bubble, Z is the freeze line height, and C and B are defined by

$$C = \pi(a_o^2 - a_i^2) \tag{5}$$

$$B = (a_o^2 - a_i^2)/2a_o^2 \tag{6}$$

where a_i and a_o are the inner and outer radii, respectively, of the die (see Fig. 1).

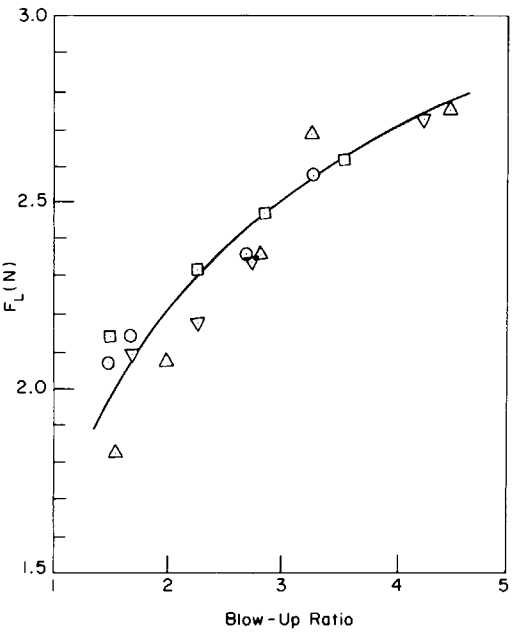

Fig. 2. Effect of blow-up ratio on the tension of the HP-LDPE bubble, at various take-up ratios: (⊙) 3.98; (△) 9.86; (⊡) 15.61; (▽) 21.44. The extrusion melt temperature is 200°C, and cooling air flow is 2210 cm^3/s.

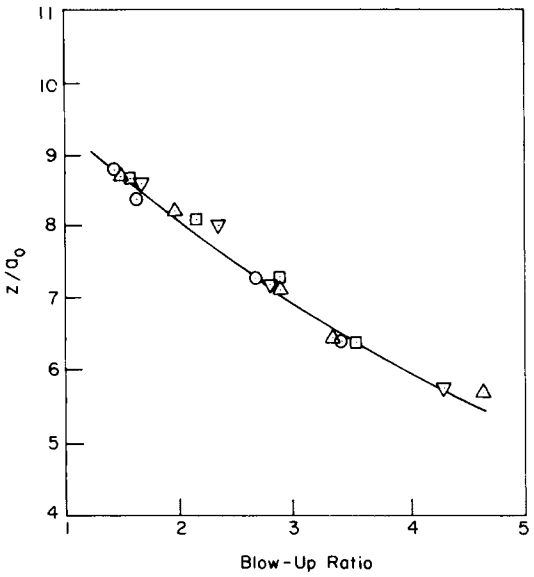

Fig. 3. Effect of blow-up ratio on the freeze-line height of the HP-LDPE bubble, at various take-up ratios: (⊙) 3.98; (△) 9.86; (⊡) 15.61; (▽) 21.44. Other processing conditions are the same as in Figure 2.

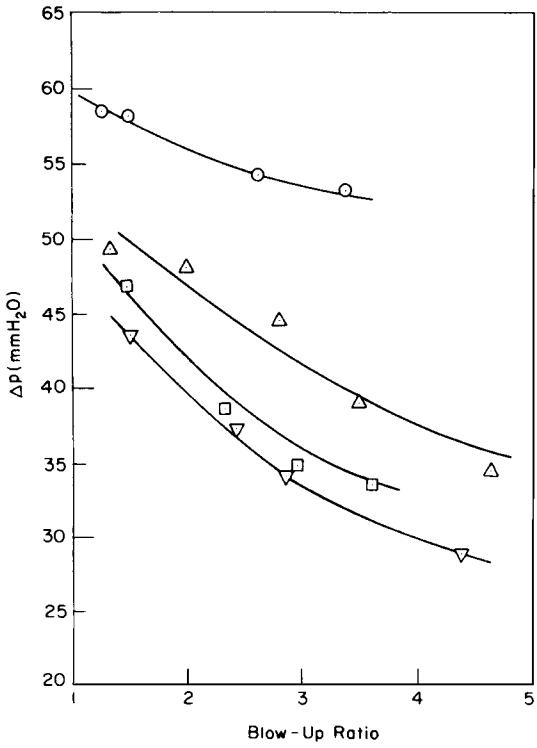

Fig. 4. Effect of blow-up ratio on the bubble pressure of the HP-LDPE, at various take-up ratios: (⊙) 3.98; (△) 9.86; (⊡) 15.61; (▽) 21.44. Other processing conditions are the same as in Figure 2.

It should be noted that F_L, Z and Δp in eqs. (3) and (4) are functions of the processing variables, namely, BUR, TUR, extrusion melt temperature, and cooling air flow rate. The effects of the variables BUR and TUR on F_L, Z, and Δp are shown in Figures 2, 3, and 4 for the HP-LDPE. Note that in Figure 3 the freeze line height is represented by the dimensionless variable, Z/a_o. Figure 2 shows that F_L increases monotonically with BUR, while Figure 3 shows that Z/a_o decreases with increasing BUR, giving rise to correlations which are less sensitive to TUR. Figure 4 describes that at a fixed TUR, Δp decreases with increasing BUR, and, at a fixed BUR, it also decreases with increasing TUR. It can therefore be predicted, using eq. (3), that S_{11F} increases not only with an increase in TUR, but also with an increase in BUR. Moreover, eq. (4) implies that S_{33F} increases at a faster rate with increasing BUR than with increasing TUR. Our results also showed that a decrease in extrusion melt temperature, and an increase in cooling flow rate, both cause an increase in F_L, a decrease in Z, and an increase in Δp. Table II gives the calculated values of S_{11F} and S_{33F} for the specimens collected in the present study.

Crystalline Structure Development as Affected by Biaxial Stresses

First, flat film methods were employed to obtain wide-angle X-ray diffraction patterns in the three principal directions. From the azimuthal dependence of the reflections, information on the orientation of the crystallographic axes was obtained. A typical wide-angle X-ray diffraction pattern of unoriented polyethylene film is shown schematically in Figure 5.

The flat plate diffraction patterns for the HP-LDPE specimens collected at different TUR's are shown in Figure 6. Each photograph was taken with the X-ray beam normal to the plane indicated on the right-hand side of each photograph. It is seen in Figure 6(a) that the (200) plane normals are randomly distributed in all directions, with somewhat higher intensity along the MD. It is also seen that the (020) poles are broadly distributed along the TD, as well as the ND, and the (110) poles are distributed in all directions with somewhat higher intensity along the TD and ND. On the other hand, it is seen in Figure 6(d) that the (200) plane normals are distributed along the MD with a certain azimuthal broadness, and the (020) poles are concentrated along the TD and ND, while the (110) poles are concentrated along the axis, which lies about 57° from the MD. Transition of the azimuthal reflection of

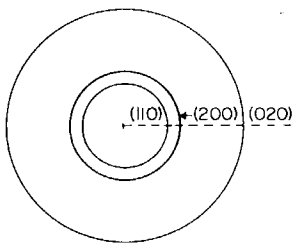

Fig. 5. Schematic of a typical wide-angle X-ray diffraction pattern of polyethylene film.

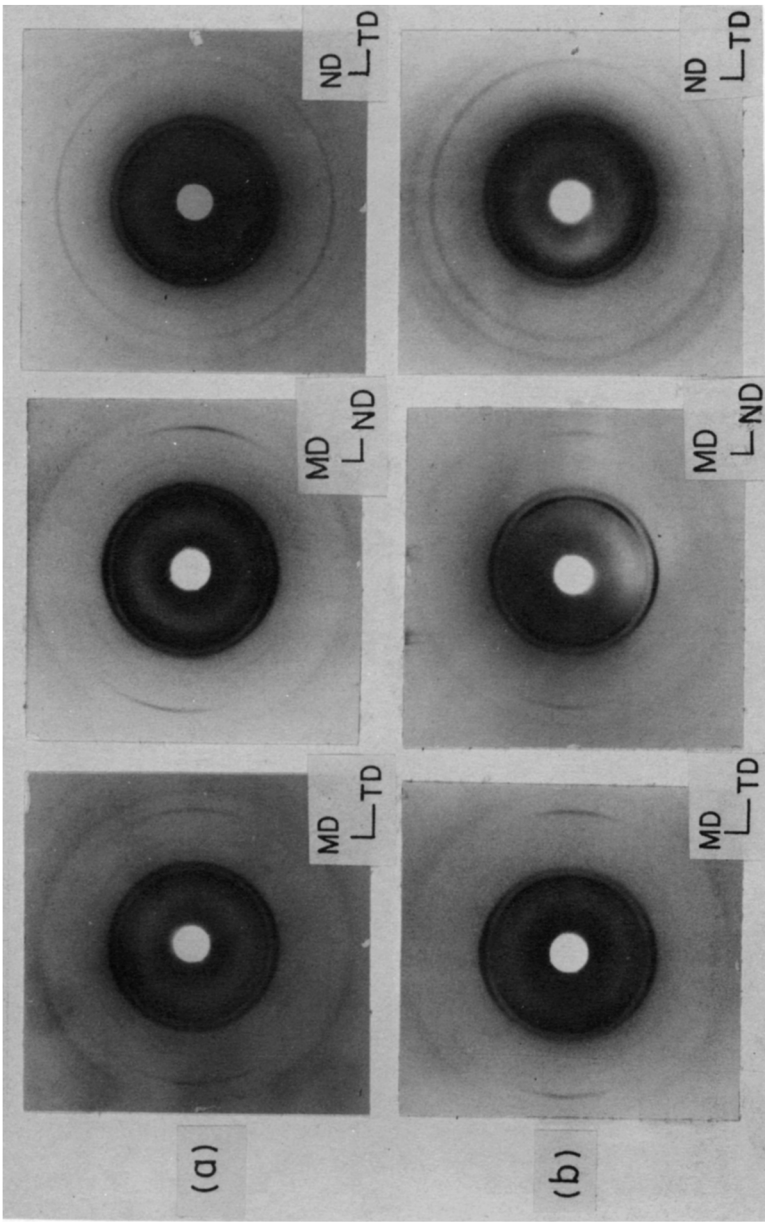

Fig. 6. Wide-angle X-ray diffraction patterns of the HP-LDPE blown films: (a) sample 3; (b) sample 5; (c) sample 6; (d) sample 9.

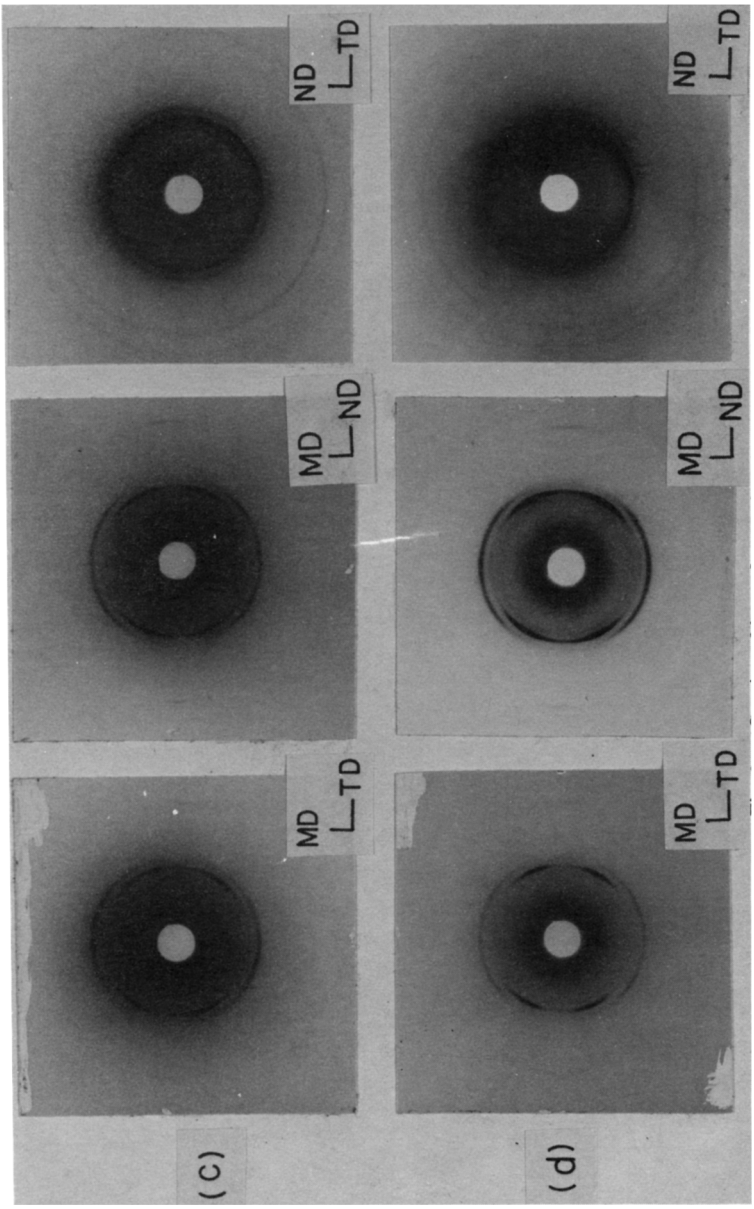

Fig. 6. *(Continued from the previous page.)*

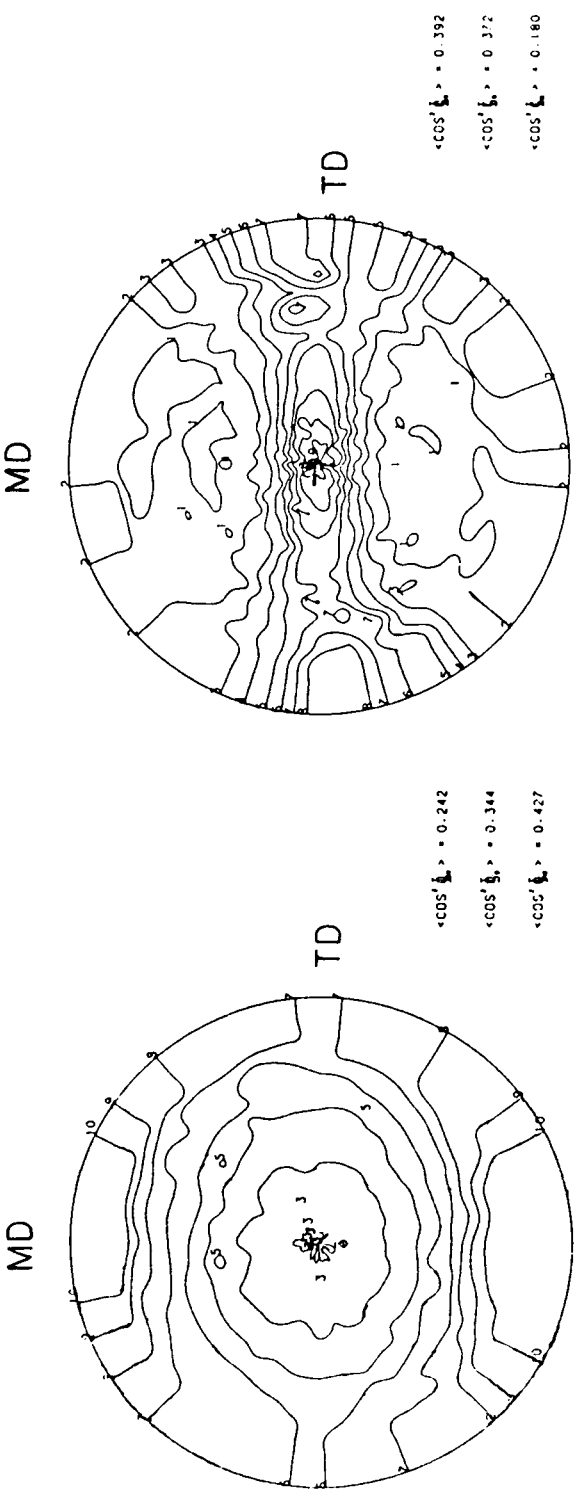

Fig. 7. Pole figures for sample 3. Left: (1) 700.5; (2) 1500.5; (3) 2200.5; (4) 3000.5; (5) 3500.5; (6) 4500.5; (7) 5300.5; (8) 6100.5; (9) 6800.5; (10) 7600.5. Right: (1) 200.5; (2) 400.5; (3) 600.5; (4) 800.5; (5) 1000.5; (6) 1200.5; (7) 1400.5; (8) 1600.5; (9) 1800.5; (10) 2000.5.

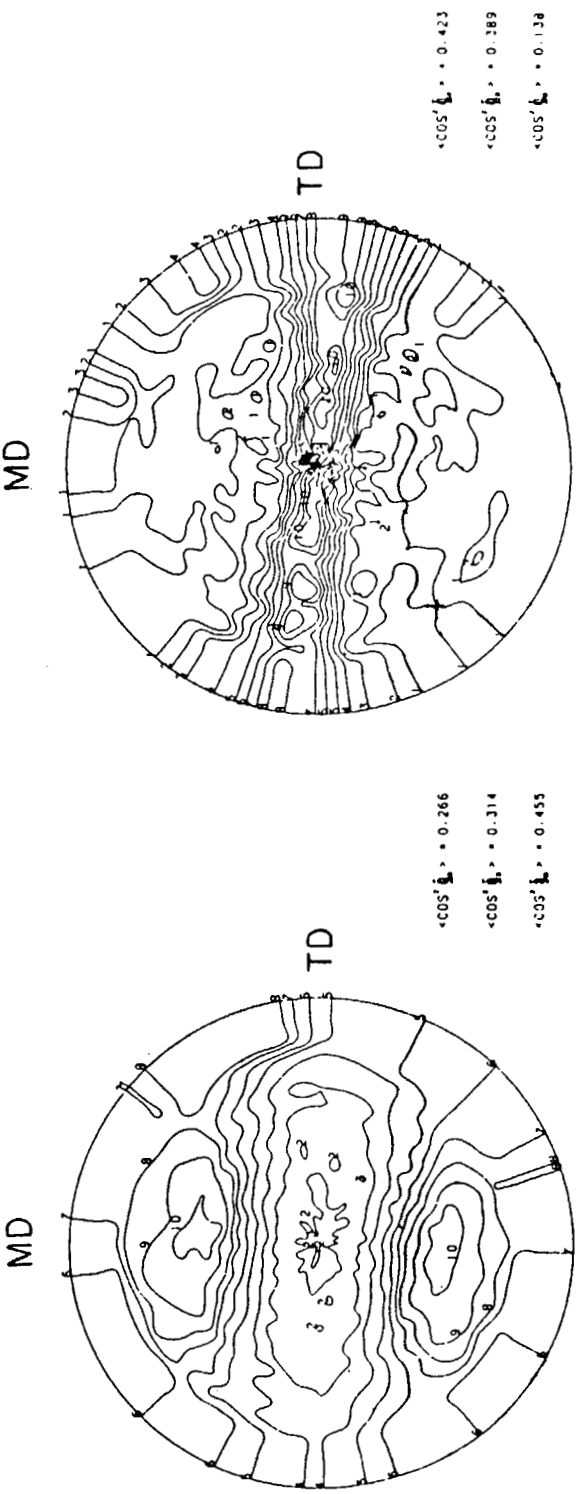

Fig. 8. Pole figures for sample 9. Left: (1) 300.5; (2) 700.5; (3) 1100.5; (4) 1400.5; (5) 1800.5; (6) 2200.5; (7) 2600.5; (8) 2900.5; (9) 3300.5; (10) 3700.5. Right: (1) 100.5; (2) 200.5; (3) 300.5; (4) 400.5; (5) 500.5; (6) 600.5; (7) 700.5; (8) 800.5; (9) 900.5; (10) 1000.5.

each plane normal can be seen from the diffraction patterns of film specimens, as shown in Figure 6(b) and 6(c).

Pole figures of (200) and (020) planes for samples 3 and 9 are given in Figures 7 and 8, respectively. Note that samples 3 and 9 have almost the same BUR, but sample 9 has a TUR much higher than sample 3 (see Table II). The following observations can be made in Figures 7 and 8: (1) the overall crystalline orientation of sample 9 is much higher than that of sample 3; (2) the contour lines of (200) reflection in sample 3 show that there is relatively little difference in intensity between the MD and TD; (3) the intensity of (020) reflection in sample 3 is broadly distributed along the plane, consisting of the TD and ND axes; (4) the (020) reflection in sample 9 has a distinctively high intensity along an axis that is between the MD and ND axes, making a certain angle with the MD; (5) the (020) reflection in sample 9 shows a high intensity along the equatorial zone with virtually little or no intensity along the MD axis. On the basis of these observations, we can conclude that the *a*- and *b*-axes in sample 3 are rather randomly distributed with their preferential direction toward the MD and the ND, respectively, whereas in sample 9 the *a*-axis is oriented along an axis between the MD and ND axes, and the *b*-axis in the ND.

In order to facilitate our discussion of crystalline axes' orientation with respect to the processing parameters S_{11F} and S_{33F} are plotted against TUR in Figure 9, for the four blown film specimens whose diffraction patterns were

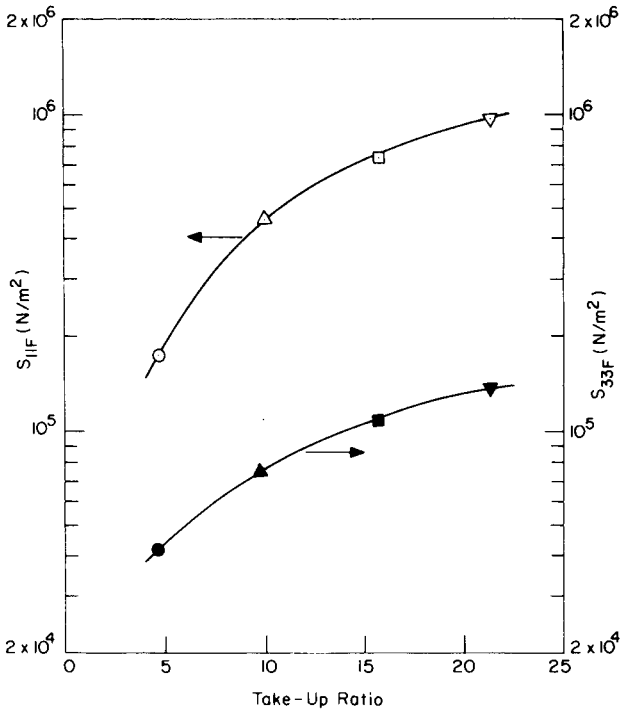

Fig. 9. S_{11F} and S_{33F} vs. take-up ratio for the HP-LDPE blown films: (⊙, ●) sample 3; (△, ▲) sample 5; (□, ■) sample 6; (▽, ▼) sample 9. Processing conditions for each sample are described in Table II.

shown in Figure 6. It is seen that both S_{11F} and S_{33F} increase with TUR and that S_{11F} is much greater than S_{33F}. The markedly different flat plate diffraction patterns (see Fig. 6), and pole figures (see Figs. 7 and 8), between samples 3 and 9 can be attributed to the difference on their S_{11F} values. We can conclude that the role of S_{33F} is very small compared to that of S_{11F}, as far as influencing the crystalline axes' orientation is concerned. More specifically, we observe that when the biaxial stress ratio, S_{11F}/S_{33F}, is much greater than unity, the variation of S_{11F} appears to play a dominant role in the development of crystalline axes orientation. This can be evidenced further from the

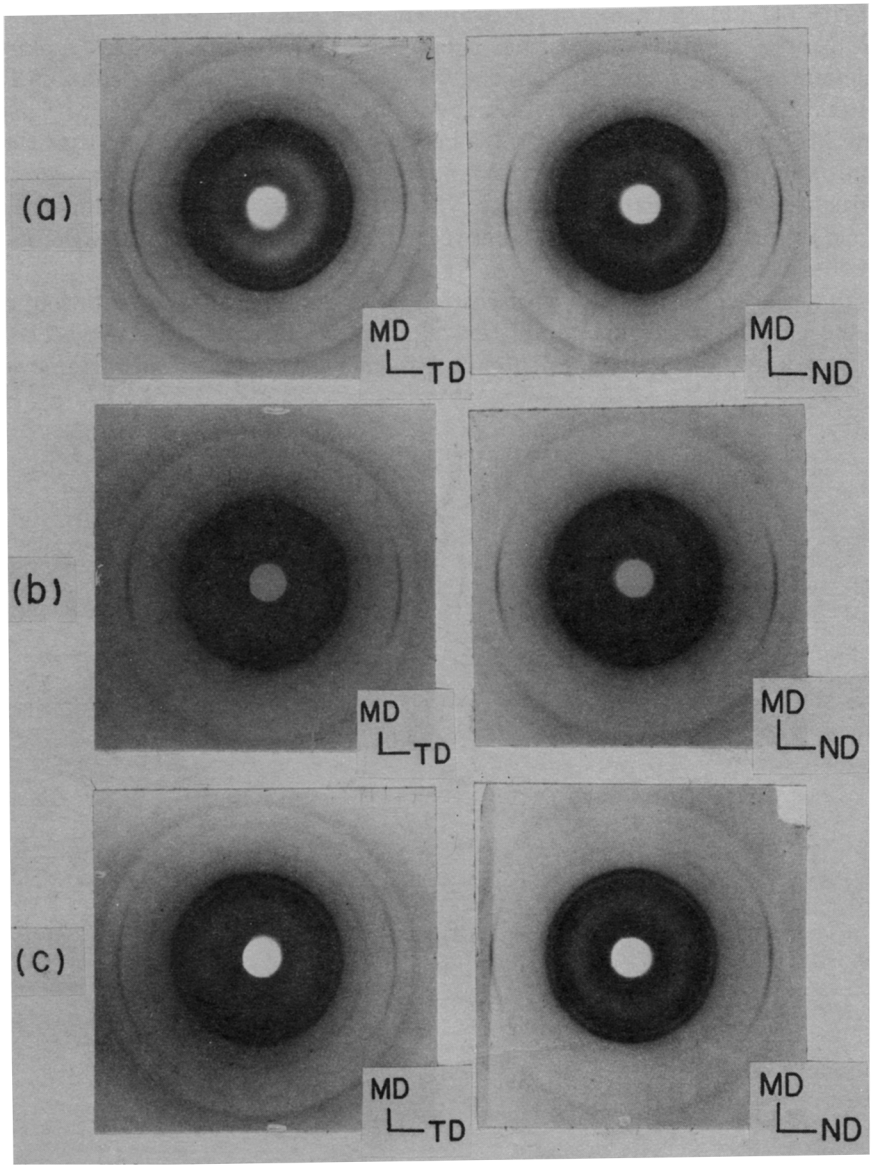

Fig. 10. Wide-angle X-ray diffraction patterns of the HP-LDPE blown films: (a) sample 1; (b) sample 2; (c) sample 4.

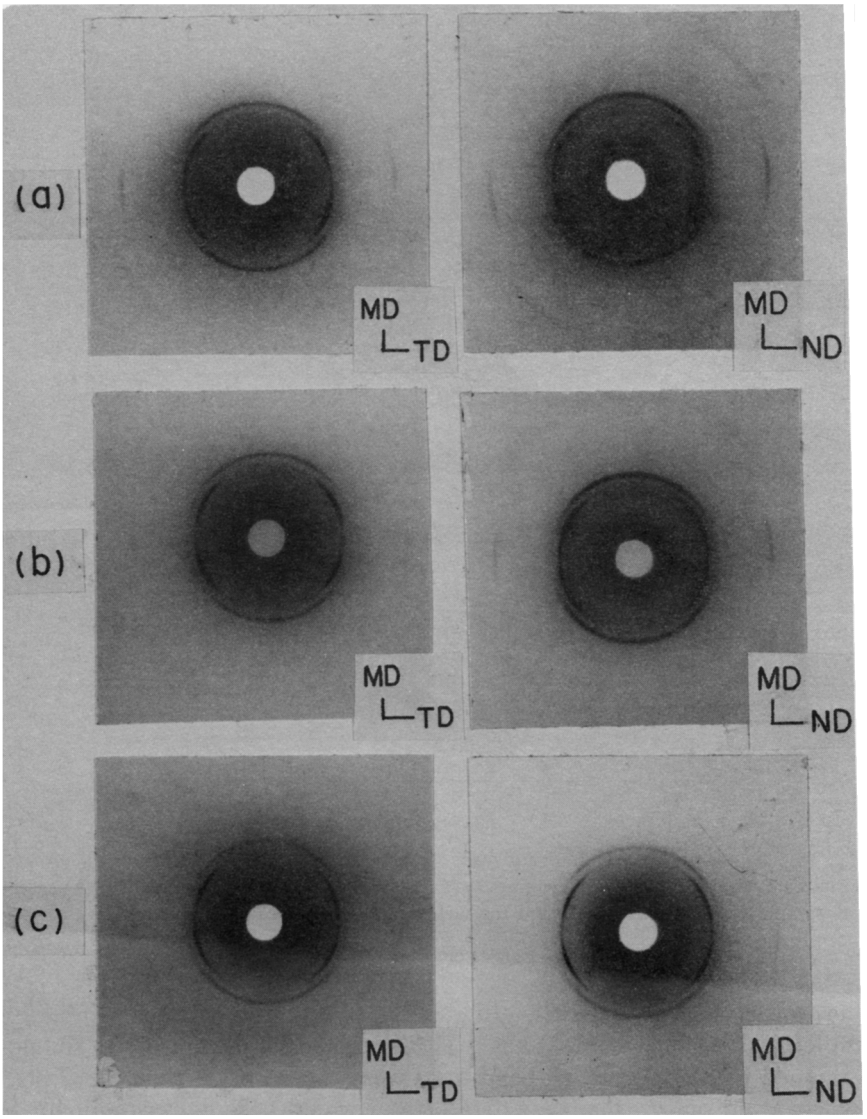

Fig. 11. Wide-angle X-ray diffraction patterns of the HP-LDPE blown films: (a) sample 7; (b) sample 8; (c) sample 10.

flat plate diffraction patterns given in Figures 10 and 11. It is seen in these figures that an increase in BUR influences little the diffraction patterns of blown film samples. It can be seen in Figure 12 that an increase in BUR has a negligible effect on the magnitude of S_{11F}. Note further that the increase in S_{33F} with increasing BUR, observed in Figure 12, has *virtually* no effect on the crystalline axes orientation. This is attributable to the fact that the magnitude of S_{11F} is much larger than that of S_{33F}. This observation is supported by the pole figures of (200) and (020) planes for sample 7, given in Figure 13, and the pole figures of (200) and (020) planes for sample 9, given in Figure 8. In

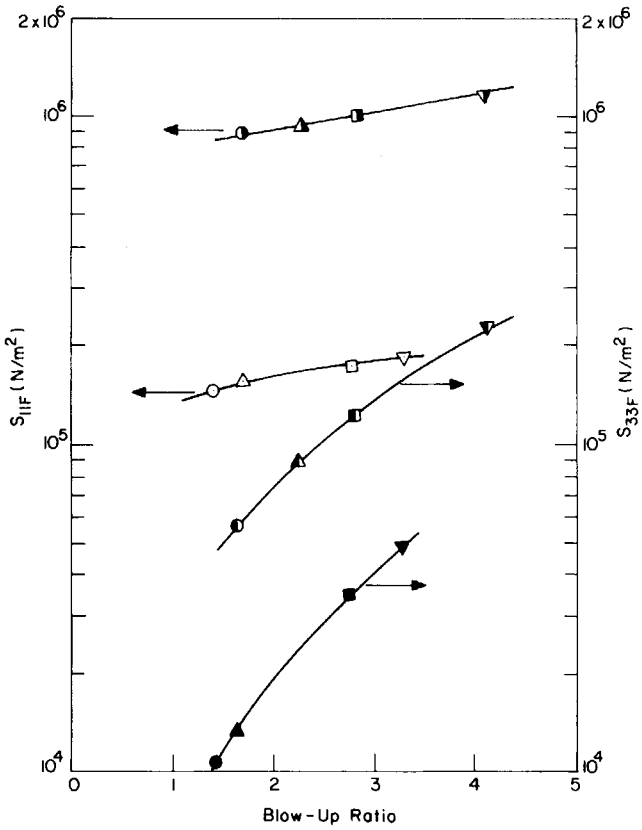

Fig. 12. S_{11F} and S_{33F} vs. blow-up ratio for HP-LDPE samples: (⊙, ●) sample 1; (△, ▲) sample 2; (⊡, ■) sample 3; (▽, ▼) sample 4; (◐, ◑) sample 7; (▲, ▲) sample 8; (◧, ◨) sample 9; (▼, ▼) sample 10. Processing conditions for each sample are described in Table II.

other words, there is very little difference in pole figures between sample 7 and sample 9, although sample 9 has a BUR larger than sample 7. It should be mentioned that if processing conditions were chosen, such that the S_{11F}/S_{33F} was less than unity, then the effect of S_{33F} would become predominant over that of S_{11F}, in influencing the crystalline axes' orientation.

A sequence of H_v small-angle light scattering patterns of four HP-LDPE blown film specimens are shown in Figure 14. It is seen from all the scattering patterns that the intensity is greatest in the center and decreases as the scattering angle decreases. Although these patterns show some diffuse scattering, the intensity of scattering along the polarizer and analyzer directions is reduced through the series of Figures 14(a)–14(d). Thus, appreciable scattering patterns of x-type are observed in Figures 14(c) and 14(d). The emergence of x-type scattering patterns [Figs. 14(c) and 14(d)] is indicative of the development of a rodlike superstructure oriented along the stretching directions,[27] i.e., MD and TD. Referring to Table II, it is clear that the rodlike superstructure becomes more pronounced as the elongational stresses imposed on the bubble during fabrication increase. As can be inferred from Figures

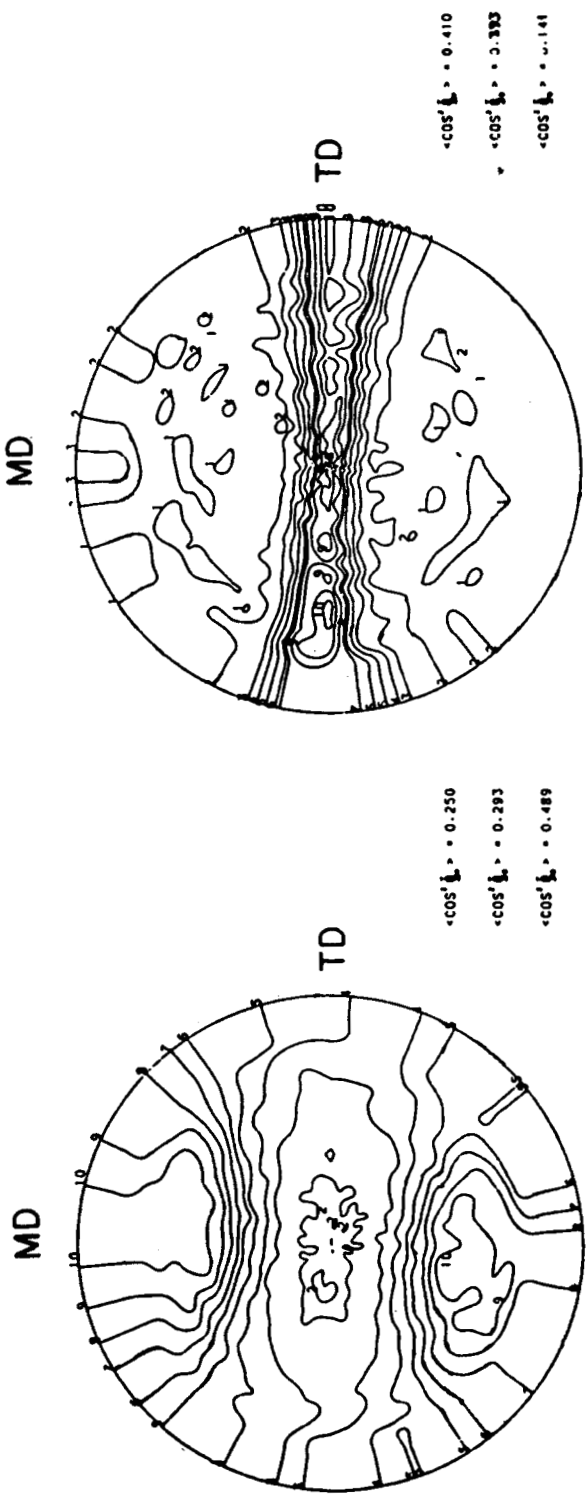

Fig. 13. Pole figures for sample 7. Left: (1) 500.5; (2) 1000.5; (3) 1600.5; (4) 2100.5; (5) 2700.5; (6) 3200.5; (7) 3700.5; (8) 4300.5; (9) 4800.5; (10) 5400.5. Right: (1) 100.5; (2) 300.5; (3) 500.5; (4) 700.5; (5) 900.5; (6) 1100.5; (7) 1200.5; (8) 1400.5; (9) 1600.5; (10) 1800.54.

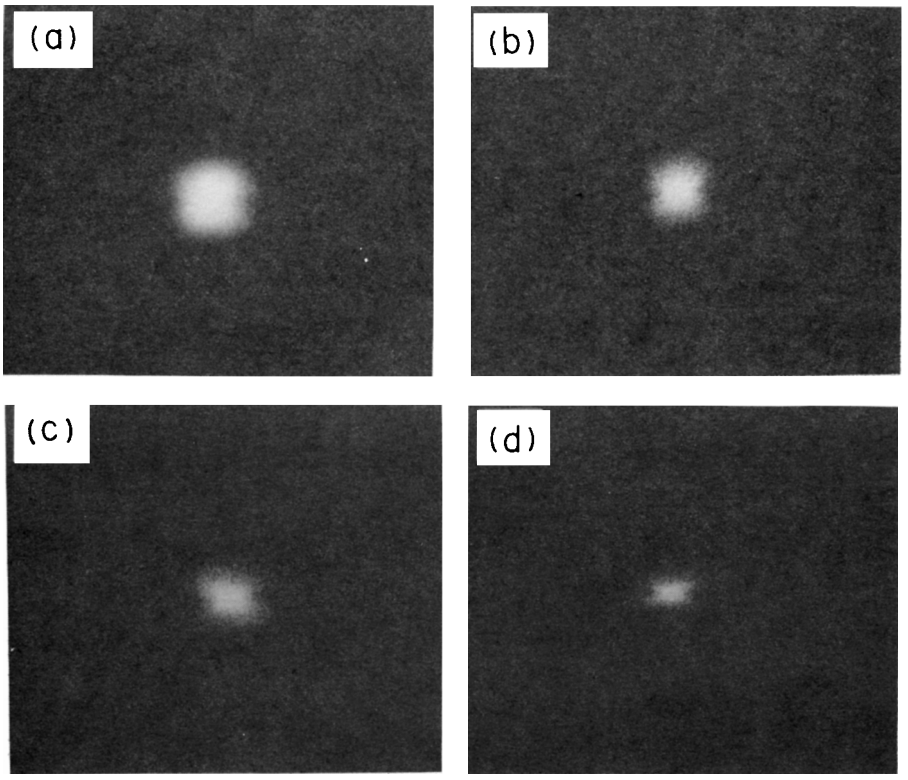

Fig. 14. H_v small-angle light scattering patterns of the HP-LDPE blown films produced at representative processing conditions (see Table II for details): (a) sample 3; (b) sample 5; (c) sample 6; (d) sample 9. MD is vertical and TD is horizontal.

14(c) and 14(d), the rodlike superstructure is aligned preferentially towards the MD, along which higher stress has been applied.

The morphology of the bulk structure of the blown film samples was examined, using scanning electron microscopy (SEM). Specimens were immersed in liquid nitrogen for about 10 min. After the specimens were completely frozen, they were fractured along the major axes. The specimens thus prepared were brittle enough to permit us to cut them easily in the specific directions desired. Figure 15 shows SEM photomicrographs of the cross section of samples 3 and 9, respectively. Note that both photomicrographs in Figure 15 represent the areas close to the edges of the cross section. Figure 15(a) shows that the microstructure in sample 3 consists of aggregates of spherulites, showing no preferential orientation. However, Figure 15(b) shows that sample 9 has a rodlike superstructure, consisting of many rods of intermediate size that are oriented preferentially in the MD. It should be remembered that sample 9 has a much higher TUR than sample 3 (see Table II). This observation was confirmed by an independent measurement, using the small-angle light scattering technique.

On the basis of the above observations, we can conclude that at a low stress state, say at and below about 10^5 N/m^2, the crystalline structure of HP-LDPE blown films is spherulitic, regardless of the value of S_{11F}/S_{33F}. However, at a

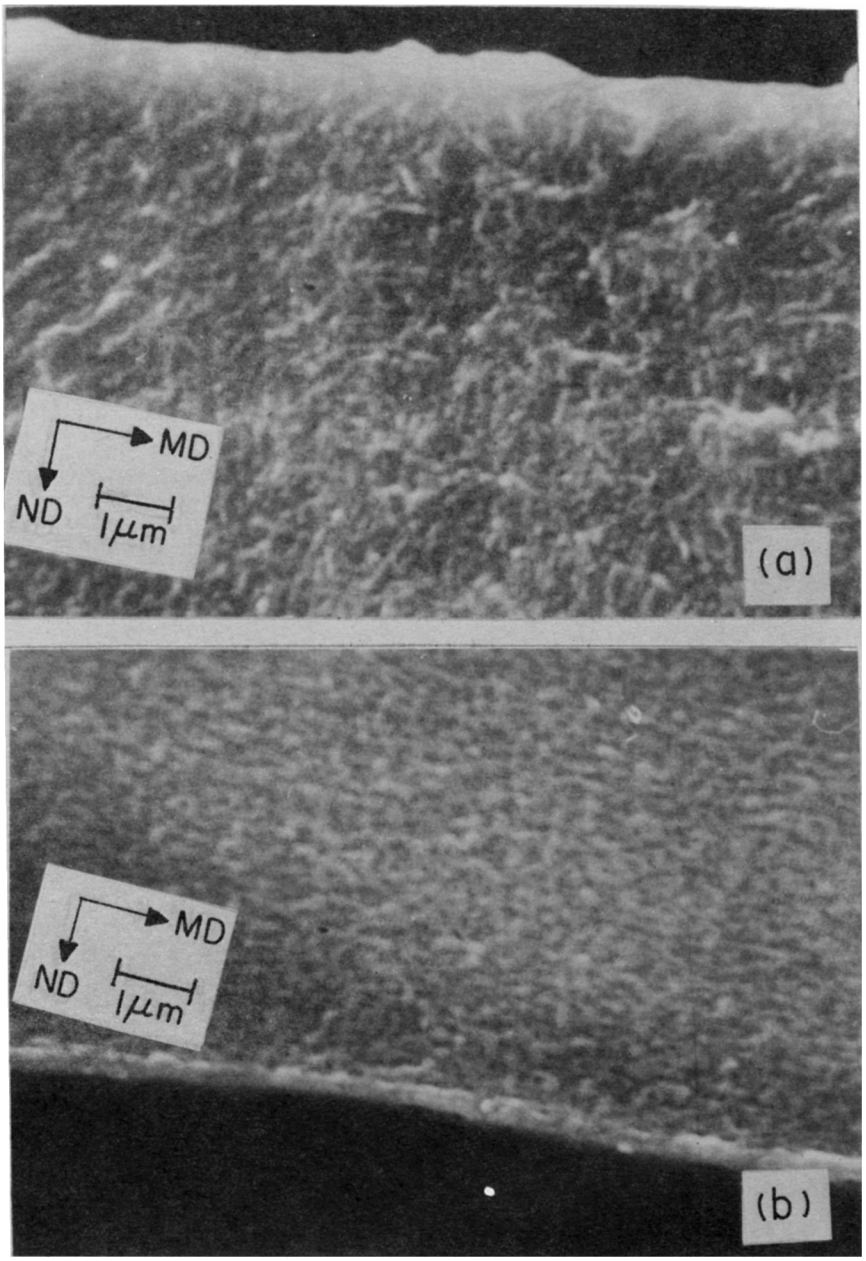

Fig. 15. SEM photomicrographs of the MD cross section of HP-LDPE blown film samples: (a) sample 3; (b) sample 9.

high stress state, a rodlike structure can be achieved. We believe that the "row structure" model for high stress state, proposed by Keller and Machin,[18] could be valid when the magnitude of applied stress exceeds about 10^7 N/m^2. This level of stress can be achieved by stretching the film samples at room temperature. None of our blown film samples showed the "row structure," even at the highest value of stress applied (ca. 10^6 N/m^2). The reason is that

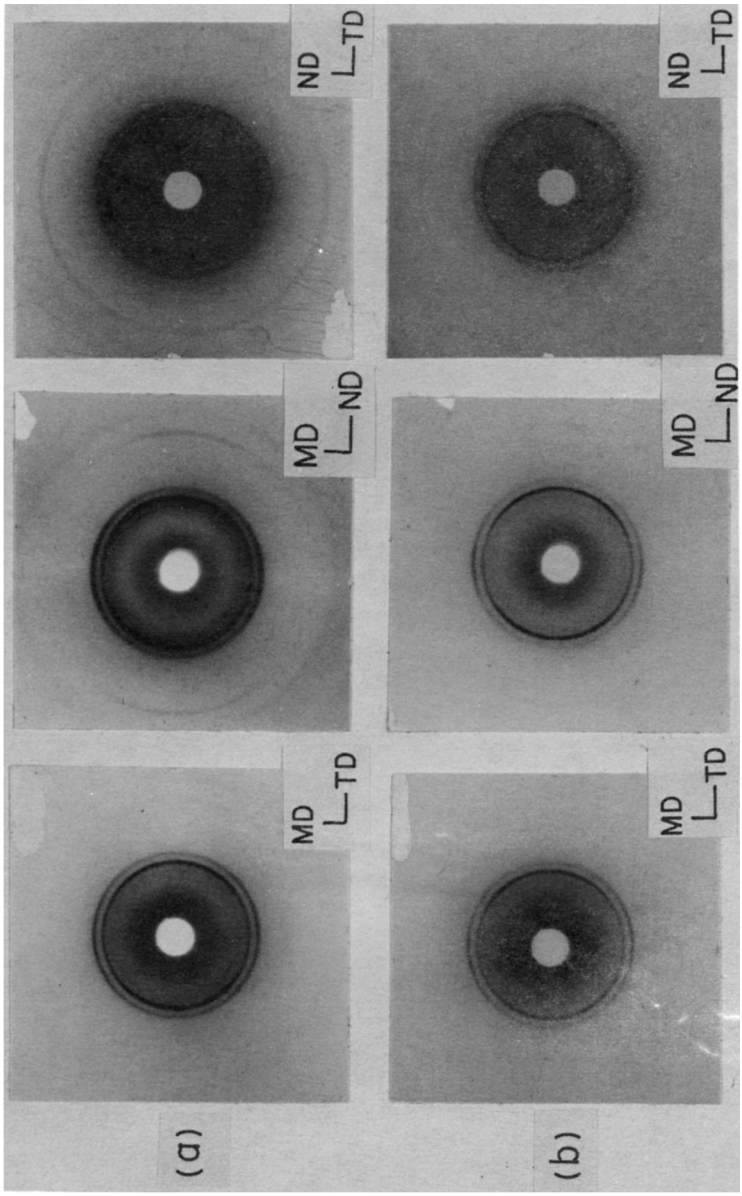

Fig. 16. Wide-angle X-ray diffraction patterns of the LLDPE blown films: (a) sample 11; (b) sample 12; (c) sample 13; (d) sample 14.

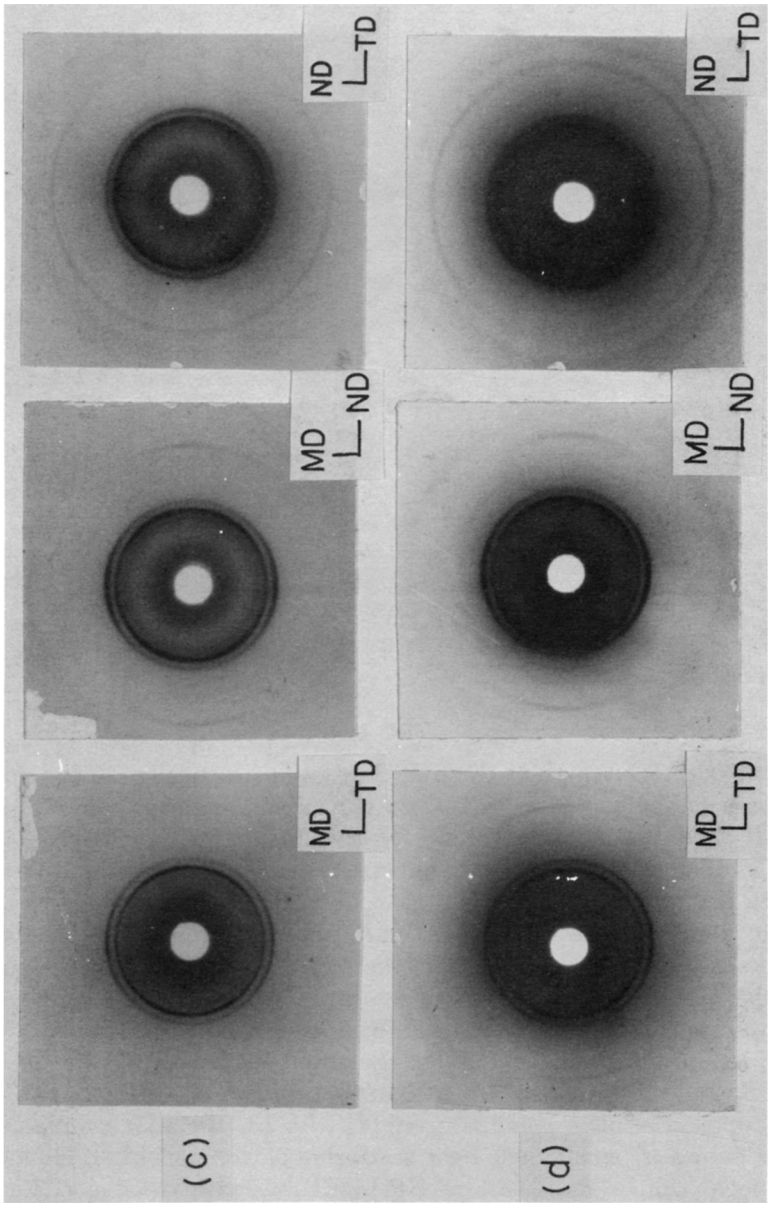

Fig. 16. *(Continued from the previous page.)*

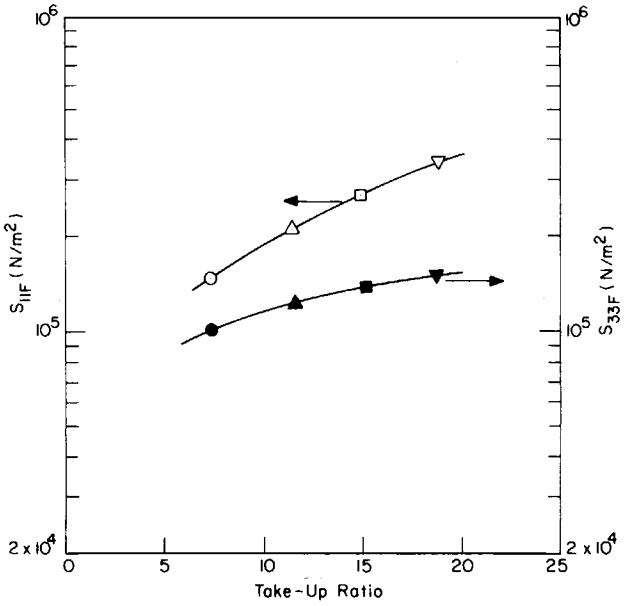

Fig. 17. S_{11F} and S_{33F} vs. take-up ratio for the LLDPE blown films (⊙, ●) sample 11; (△, ▲) sample 12; (⊡, ■) sample 13; (▽, ▼) sample 14. Processing conditions for each sample are described in Table II.

the rather weak melt strength of HP-LDPE makes it practically impossible to apply a stress as high as 10^7 N/m^2 to a tubular bubble during film blowing operation. It should be mentioned, however, that Maddams and Preedy[15] and Maddams and Vickers[22] observed high stress orientation in some of the high-density polyethylene films that they examined.

Let us now discuss our results on LLDPE blown film samples. The effects of TUR on the flat plate diffraction patterns of the LLDPE, taken at three perpendicular directions, are shown in Figure 16. Azimuthal dependency of each reflection pattern on TUR for LLDPE is less conspicuous than that for HP-LDPE. Again, this is due to the fact that the magnitude and the rate of increase of S_{11F} in the LLDPE is lower than that in the HP-LDPE. Figure 17 shows the dependence of S_{11F} and S_{33F} on TUR for LLDPE film samples.

Figure 18 shows H_v small-angle light scattering patterns of LLDPE blown film specimens. Unlike those of the HP-LDPE specimens, these patterns indicate that LLDPE samples 11 and 14 have a spherulite-like structure. Although the scattering patterns are hazy and diffuse, the patterns in Figure 18(a) might have arisen from the presence of a sheaf-like superstructure[28] and Figure 18(b) from ellipsoidal spherulites. Light scattering patterns of LLDPE samples 12 and 13, though not shown here due to space limitations, show patterns intermediate between the two shown in Figure 18. A comparison of Figure 14 with Figure 18 reveals that the variation of crystalline structure is less conspicuous in LLDPE than in HP-LDPE, which was also revealed by the orientation of the crystalline axes observed with flat plate diffraction patterns discussed above.

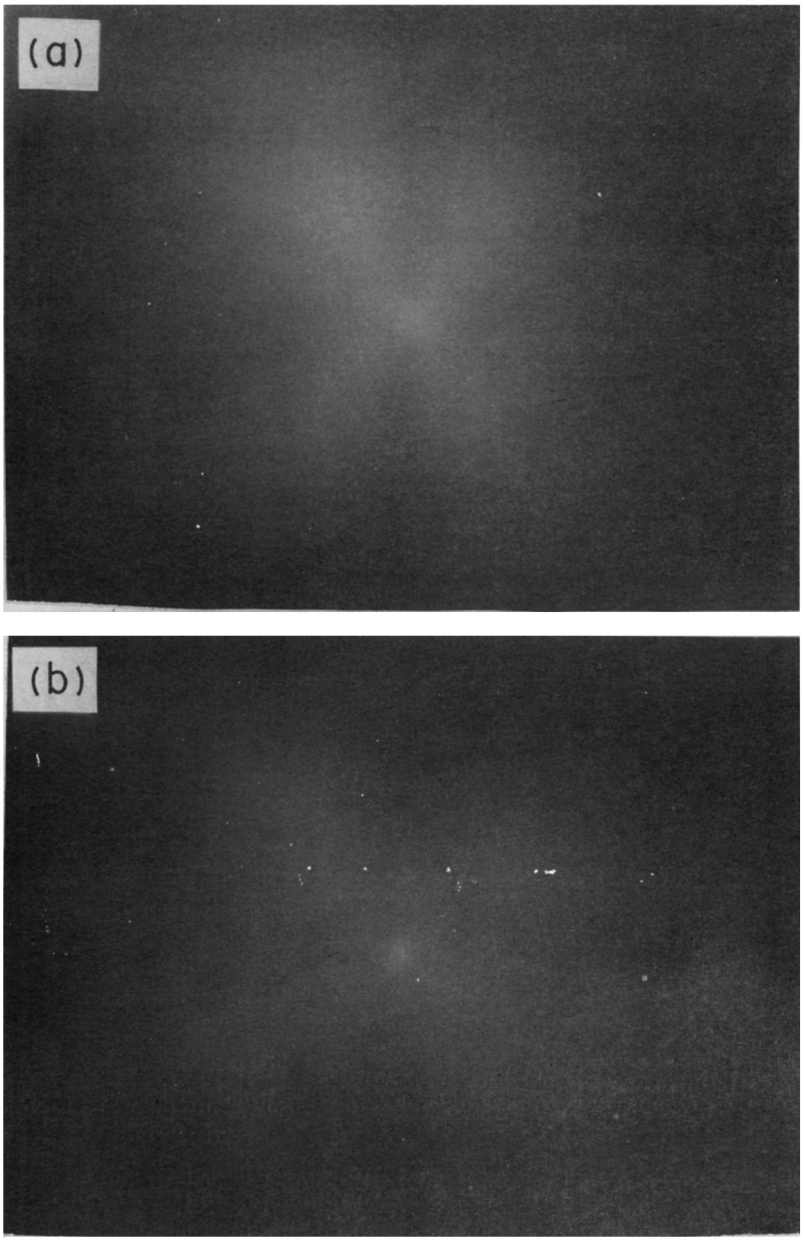

Fig. 18. H_v small-angle light scattering patterns of the LLDPE blown films produced at different processing conditions (see Table II): (a) sample 11; (b) sample 14. MD is vertical and TD is horizontal.

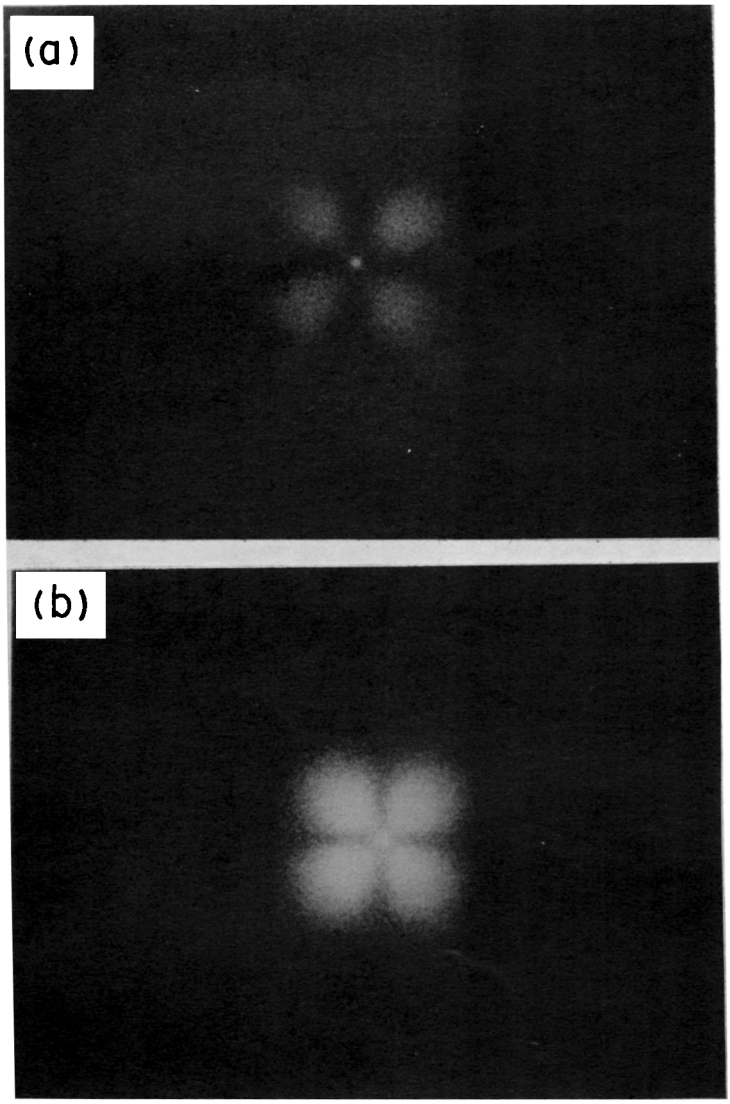

Fig. 19. H_v small-angle light scattering patterns of low-density polyethylene crystallized from unstressed melts: (a) HP-LDPE; (b) LLDPE.

The small-angle light scattering patterns of thermally controlled film specimens crystallized from an unstressed melt state are shown in Figure 19. The two resins employed in this study were inserted between two microslides and then inserted in a hot stage. The temperature of the hot stage was increased to 190°C at a rate of 10°C/min, held at 190°C for 5 min and then cooled to room temperature at a rate of 10°C/min. It is seen from Figure 19 that both specimens have well-developed spherulitic structure.

The results shown above illustrate that, although the two resins show a similar crystalline structure when prepared from a quiescent melt state, the crystalline structure of two different kinds of blown film specimens produced at comparable processing conditions differ from each other. The distinct

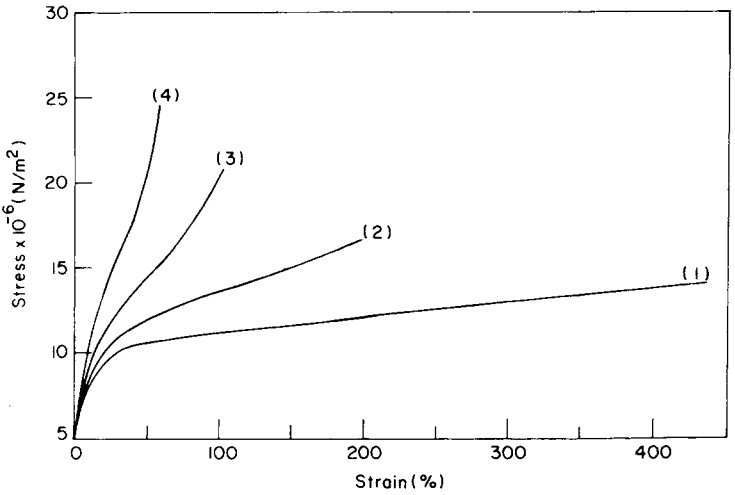

Fig. 20. Normalized stress–strain curves along the MD for the HP-LDPE blown films: (1) sample 3; (2) sample 5; (3) sample 6; (4) sample 9.

difference between HP-LDPE films and LLDPE films, in the development of morphology, can be attributed to the dissimilarity of stress histories during the expansion of the bubble. This implies that the rheological response of a resin to the processing variables plays a significant role in determining the resultant film morphology. Thus, for LLDPE the imposition of relatively low biaxial stresses and a low value of their ratio, as shown in Table II, seem to bring about a more or less spherulitic structure. Consequently, it can be concluded that structural development cannot be described solely by the use of BUR or TUR. Instead, one must use the magnitude and direction of stresses as process parameters, which are the rheological responses to deformation. Thus, when the level of stresses is known either by measurement or simulation, it will be possible for one to predict the resultant film morphology.

Tensile and Dynamic Mechanical Properties of the Blown Films

Tensile properties were measured at room temperature, and normalized curves of stress-strain in the MD are shown in Figure 20 for the four blown samples of HP-LDPE. It is seen that, as the TUR increases at a fixed BUR, the tensile modulus, yield stress, and ultimate tensile strength increase, while both the elongation at yield and the elongation at break decrease. Since cold drawing is involved after the yield point, a structural transition has taken place during the test. Thus, only the slope of the initial curve (i.e., the tensile modulus) can be attributed to the structure of the as-blown films. Consequently, it can be concluded that a blown film having a "rodlike structure" has a higher tensile modulus in the MD. However, any quantitative consideration of the structure–property relationship would require information on the structure in the amorphous region between lamellae, i.e., the number of tie molecules.

The elastic modulus (E') and loss tangent ($\tan \delta$) of the four blown film samples in the MD are plotted against temperature in Figure 21. It is seen

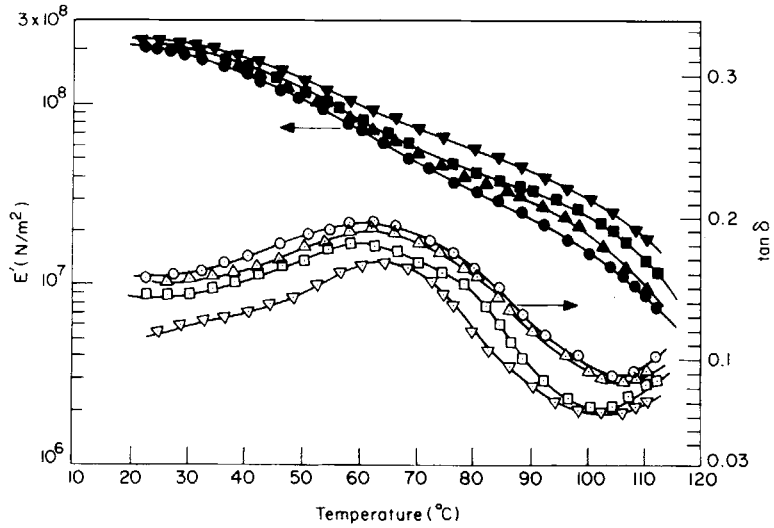

Fig. 21. Dynamic modulus and the dynamic loss tangent (tan δ) along the MD for the HP-LDPE blown films: (⊙, ●) sample 3; (△, ▲) sample 5; (⊡, ■) sample 6; (▽, ▼) sample 9.

that the E' of sample 9 is the highest and that of sample 3 the lowest, over the range of temperature investigated. The broad peak seen in the tan δ curve between the glass transition temperature and the melting temperature is termed the α' peak. The origin of the α' peak is not clearly understood, yet. Kawai et al.[29] attributed this peak to an intralamellar grain boundary phenomenon, such as lamellar untwisting and lamellar tilting, while Popli et al.[30] found this peak to be dependent primarily upon crystallite thickness.

In the present case, we speculate that the α' peak originates from the relaxation of twisted lamellae to a less ordered state. It is seen from Figure 21 that the α' peak has a tendency to increase slightly with increasing TUR. It may be that a greater energy is required for relaxation to occur in sample 9, since it has a "rodlike structure" in which lamellae would exist in a more ordered state than in other samples.

CONCLUDING REMARKS

We have concluded that the biaxial stress ratio, S_{11F}/S_{33F}, is an important rheological parameter that decides the relative importance between the two directional stresses, S_{11F} and S_{33F}, and can be used to determine the distribution of fibrillous nuclei, which influences the crystalline texture and, thus, the film anisotropy. When the S_{11F}/S_{33F} ratio is greater than unity, the magnitude of the principal stress, S_{11F}, was found to play a dominant role in influencing the crystalline axes' orientation.

It is suggested that an investigation be made of the amorphous region with respect to the processing parameters, as well as the role of tie molecules in influencing the mechanical or physical properties of blown films. It is also suggested that the effects of molecular parameters (i.e., the degree of long-chain branching) on the crystallization behavior and, possibly, on the formation of tie molecules between lamellae be investigated.

References

1. J. R. A. Pearson and C. J. S. Petrie, *J. Fluid Mech.*, **40**, 1 (1970); **42**, 609 (1970).
2. J. R. A. Pearson and C. J. S. Petrie, *Plast. Polym.*, **38**, 85 (1970).
3. R. Farber and J. Dealy, *Polym. Eng. Sci.*, **14**, 435 (1974).
4. C. D. Han and J. Y. Park, *J. Appl. Polym. Sci.*, **19**, 3257, 3277 (1975).
5. S. C. K. Chung and J. F. Stevenson, *Rheol. Acta*, **14**, 832 (1975).
6. C. D. Han and R. Shetty, *Ind. Eng. Chem. Fundam.*, **16**, 49 (1977).
7. C. D. Han and J. Y. Park, *J. Appl. Polym. Sci.*, **19**, 3291 (1975).
8. N. D. Huck and P. L. Clegg, *Soc. Plast. Eng. Trans.*, **1**(3), 121 (1961).
9. V. G. Kendall, *Trans. Plast. Inst.*, **31**(2), 49 (1963).
10. D. R. Holmes and R. P. Palmer, *J. Polym. Sci.*, **31**, 345 (1958).
11. S. L. Aggarwal, G. P. Tilley, and O. J. Sweeting, *J. Appl. Polym. Sci.*, **1**, 91 (1959).
12. P. H. Lindenmeyer and S. Lustig, *J. Appl. Polym. Sci.*, **9**, 227 (1965).
13. C. R. Desper, *J. Appl. Polym. Sci.*, **13**, 169 (1969).
14. T. Nagasawa, T. Matsumura, S. Hoshino, and K. Kobayashi, *Appl. Polym. Symp.*, **20**, 275, 295 (1973).
15. W. F. Maddams and J. E. Preedy, *J. Appl. Polym. Sci.*, **22**, 2721 (1978).
16. W. F. Maddams and J. E. Preedy, *J. Appl. Polym. Sci.*, **22**, 2739 (1978).
17. W. F. Maddams and J. E. Preedy, *J. Appl. Polym. Sci.*, **22**, 2751 (1978).
18. A. Keller and M. J. Machin, *J. Macromol. Sci. Phys.*, **B1**, 41 (1967).
19. K. J. Choi, J. E. Spruiell, and J. L. White, *J. Appl. Polym. Sci.*, **25**, 2777 (1980).
20. K. J. Choi, J. E. Spruiell, and J. L. White, *J. Polym. Sci., Polym. Phys. Ed.*, **20**, 27 (1982).
21. Y. Shimomura, J. E. Spruiell, and J. L. White, *J. Appl. Polym. Sci.*, **27**, 2663 (1982).
22. W. F. Maddams and M. E. Vickers, *J. Elast. Plast.*, **15**, 246 (1983).
23. H. Ashizawa, J. E. Spruiell, and J. L. White, *Polym. Eng. Sci.*, **24**, 1035 (1984).
24. C. D. Han and T. H. Kwack, *J. Appl. Polym. Sci.*, **28**, 3399 (1983).
25. T. H. Kwack and C. D. Han, *J. Appl. Polym. Sci.*, **28**, 3419 (1983).
26. R. S. Stein, in *Structure and Properties of Polymer Films*, R. W. Lenz and R. S. Stein, Eds., Plenum, New York, 1973.
27. R. J. Samuels, *Structured Polymer Properties*, Wiley, New York, 1974.
28. T. Hashimoto, A. Todo, Y. Murakami, and H. Kawai, *J. Polym. Sci.*, **15**, 501 (1977).
29. H. Kawai, T. Hashimoto, S. Senhiro, and K. Fujita, *Polym. Eng. Sci.*, **24**, 361 (1984).
30. R. Popli, M. Glotin, and L. Mandelkern, *J. Polym. Sci., Polym. Phys. Ed.*, **22**, 407 (1984).

Received March 3, 1984
Accepted May 15, 1987